

ARTICLES

Size and Band-Gap Dependences of the First Hyperpolarizability of Cd_xZn_{1-x}S Nanocrystals

D. V. Petrov,* B. S. Santos, G. A. L. Pereira, and C. de Mello Donegá

*Departamento de Química Fundamental, Universidade Federal de Pernambuco, 50670-901 Recife, PE, Brazil**Received: February 16, 2001; In Final Form: January 16, 2002*

The first hyperpolarizability of aqueous suspensions of polyphosphate stabilized CdS nanocrystals of different mean sizes and of Cd_xZn_{1-x}S nanocrystals ($x = 0, 0.25, 0.75, 1$) was determined by the hyper-Rayleigh scattering technique. We report the first experimental observation that the first hyperpolarizability decreases as the band gap energy increases. This is ascribed to the decrease of the resonance enhancement. The surface modification of 9 nm CdS nanocrystals with OH⁻ increases the first hyperpolarizability by a factor 1.7. This is explained in terms of the higher polarizability of the surface terminating groups after the OH⁻ modification. Finally, we have also established the size dependence of the first hyperpolarizability for CdS nanocrystals. Although it increases with the particle size, its values normalized per CdS pair increase with decreasing of size, leading to an enhancement by 1 order of magnitude for 2 nm particles in comparison with bulk. This is explained by assuming the enhancement of both the bulk contribution from the noncentrosymmetric nanocrystal core and the surface contribution. The enhancement of the bulk contribution is ascribed to quantum confinement effects on the normalized oscillator strengths. The surface contribution becomes more relevant as the size decreases and may be enhanced by several effects, especially surface polarization. A two-level model can explain both the band-gap and the size dependences.

1. Introduction

Low dimensional structures and nanostructured materials have attracted great interest in recent years because their properties are markedly different from those of bulk materials. These differences arise from several phenomena (viz. quantum confinement of electrons and holes, surface effects, and geometrical confinement of phonons), which play different roles depending on the investigated property.¹⁻³ Therefore, one can use materials with already desirable bulk properties and improve or tailor these properties by a judicious control of size and surface.¹⁻³ A semiconductor nanoparticle is an example of a low-dimensional structure. The nanoparticle has a rather large number of atoms, but its size is comparable with characteristic dimensions describing the behavior of electrons and holes, thus creating an intermediate regime between molecules and bulk crystals.¹⁻³

Semiconductor nanostructures are considered as promising materials for several applications.¹⁻⁷ The availability of large nonlinear optical coefficients in these materials may lead to photonics applications, such as ultrafast optoelectronic switches. Moreover, nonlinear optical processes may provide valuable information for proper understanding of quantum confinement and surface effects in low-dimensional structures. For this reason, the optical properties of semiconductor nanocrystals suspended or embedded in many different media have been extensively investigated in the past decade.¹⁻³

Another possible application which has received increasing attention in recent years is in biological labeling and nanoscale

topographic localization of probes in biological systems.⁴⁻⁷ The association of near-field scanning optical microscopy (NSOM) techniques and the nonlinear (upconversion luminescence and second harmonic generation)⁴ or linear (fluorescence)⁵⁻⁷ optical properties of nanocrystals has created the exciting possibility of realizing multicolor single excitation labeling^{5,6} and dynamic three-dimensional nanoscale optical imaging.⁷ Furthermore, compared with conventional fluorophores, nanocrystalline semiconductor particles have a brighter and narrower emission and are more stable against photobleaching.^{5,6} However, a better understanding of the nonlinear and linear optical processes in semiconductor nanocrystals, as well as adequate preparation methods, are still needed in order to realize these potential applications.²⁻⁷

The spatial confinement of the charge carriers (electrons and holes) in low-dimensional systems changes both linear and nonlinear optical properties,¹⁻³ because it affects the polarization response of the material to an inducing optical field. The polarization response P is given by⁸

$$P = \alpha E + \beta E^2 + \gamma E^3 + \dots \quad (1)$$

where α is the linear polarizability, β is the first hyperpolarizability, γ is the second hyperpolarizability, and E is the inducing optical field strength.

The investigations on the nonlinear optical properties of semiconductor nanocrystals have focused mainly into the third-order optical nonlinearity (or second hyperpolarizability γ).^{1,2,9-19} A large enhancement of this optical nonlinearity because of size quantization of the exciton motion has been predicted by Nakamura et al.⁹ and by Banyai et al.¹⁰ Although some

* To whom correspondence should be addressed. E-mail: dvp@npd.ufpe.br. Phone: +55-081-3271-8440. Fax: +55-081-3271-8442.

experiments have supported this prediction,^{1,11,13} an unambiguous picture describing the size dependence of the third-order nonlinear optical susceptibility has yet to emerge.

The second-order optical nonlinearity (or the first hyperpolarizability β) of semiconductor nanoparticles has been more sparsely investigated.^{20–27} The size dependence of second harmonic generation from the surface of a composite material consisting of CdSe nanoparticles embedded in a glass matrix has been studied by Aktsipetrov et al.^{20,21} It was shown that the effective first hyperpolarizability β of a single particle averaged over the ensemble increases as $D^{5/2}$ with decreasing of the average particle diameter D within the range $5 \text{ nm} < D < 100 \text{ nm}$. This effect was explained by fluctuations of the particle shape giving rise to quantum chaotic electron dynamics.

The first hyperpolarizability of CdS nanocrystals in colloidal suspensions was studied by Lu et al.^{22–24} using a hyper-Rayleigh scattering (HRS) technique. The reported β values are among the largest observed for solution samples. The measurements were carried out on samples with two different mean particle diameters (3 and 4 nm), although the size dependence of β was not discussed.²² Moreover, differences on the β values depending on the surface of the CdS particles were reported.^{22–24}

Brysch et al.²⁵ investigated the second harmonic generation (SHG) by colloidal aqueous suspensions of CdS nanocrystals with different surface stabilizers and mean diameters ranging from 6 to 12 nm. However only the relative magnitudes of the SHG signals were reported, with no attempt being made to derive the values of the first hyperpolarizability β .²⁵ The SHG signal was observed to increase by 2 orders of magnitude with the decreasing of size and to be enhanced by up to a factor of 10 depending on the stabilizer. The SHG signal was assumed to be totally due to the surface and to deviations from spherical shape.²⁵

Recently, we reported HRS measurements for aqueous colloidal suspensions of polyphosphate stabilized CdS nanocrystals (mean diameters: 2–9 nm) that also revealed large β values.²⁶ Our results showed that, although the first hyperpolarizability β increases with the particle size, the values of β normalized per CdS pair increase with decreasing particle size. This size dependence was ascribed to quantum confinement effects on the volume normalized exciton oscillator strengths.²⁶

A similar size dependence has been recently reported by Jacobsohn and Banin²⁷ for the first hyperpolarizability of TOPO (triethylphosphineoxide) stabilized CdSe nanocrystals (mean diameters: 2.0–10.0 nm). They observed that the values of β per nanocrystal decrease with size for diameters down to 2.6 nm but increase with further size reduction. Moreover, the unit cell normalized β increases with decreasing of particle size, with a substantial enhancement (by a factor ~ 5) in diameters smaller than 4.0 nm.²⁷ The authors explained the observed size dependence by assuming that the HRS signal has both a bulklike contribution from the noncentrosymmetric nanocrystal core and a surface contribution. Quantum size effects were assumed to play no role in the enhancement of the unit cell normalized β , which was totally ascribed to surface effects.²⁷

The manifestation of quantum size effects in nonlinear optical processes depends on the electronic properties of the semiconductor, in particular, its band gap. In this work, we measured the β values by the HRS technique for four aqueous suspensions of $\text{Cd}_x\text{Zn}_{1-x}\text{S}$ nanocrystals with the same diameter (9 nm) but with different values of x and, therefore, different band gap energies. We thus report the first hyperpolarizability of semiconductor nanocrystals on the energy gap between the highest occupied

energy level and the lowest unoccupied energy level. We have also reinvestigated the β values for CdS nanocrystals of different mean diameters in order to confirm the size dependence of β , previously reported by us.²⁶ Furthermore, to evaluate the relative contribution of surface effects, we measured the β values for 9 nm polyphosphate stabilized CdS nanocrystals prior to and after their surface modification with OH^- .

2. Experimental Section

2.1. Synthesis and Characterization. Aqueous suspensions of polyphosphate stabilized nanocrystalline $\text{Cd}_x\text{Zn}_{1-x}\text{S}$ particles ($x = 0, 0.25, 0.75, 1$) were prepared by slightly modifying the well-established polyphosphate method.^{28–31} A volume of 700 μL of H_2S (White-Martins, 99.5%) was injected with an airtight syringe into the gas phase of a septum closed 250 mL flask containing 100 mL of an aqueous solution of $5.6 \times 10^{-3} \text{ M}$ sodium polyphosphate ($(\text{NaPO}_3)_n$ Aldrich, 98%) and a variable concentration of $x\text{Cd}(\text{ClO}_4)_2 \cdot 6\text{H}_2\text{O}$ and $(1-x)\text{Zn}(\text{C}_2\text{H}_4\text{O}_2)_2$ (both Aldrich, 99%), at $\text{pH} = 8.5$ and room temperature. The flasks were then vigorously shaken for 10 min and kept closed for 24 h. The particle sizes were controlled by the Cd/S ratio. For the $\text{Cd}_x\text{Zn}_{1-x}\text{S}$ suspensions, this ratio was kept at 1 ($[\text{Cd}_x\text{Zn}_{1-x}] = 2.50 \times 10^{-4} \text{ M}$). For suspensions of CdS nanocrystals of different sizes, the Cd/S ratios were set at 1.0, 1.6, and 4.0. The size distributions of the nanoparticles prepared by this method are expected to have a standard deviation of $\sim 15\%$.^{28–32}

The surface modification of the CdS nanocrystals with OH^- (a process better known as passivation^{29,32}) was carried out on samples with $\text{Cd/S} = 1$, following the method reported in the literature,^{29,32} which consists on rising the pH of the CdS suspension to 10.5 by dropwise addition of NaOH 0.1 M, followed by the dropwise addition of ca. 6 mL of a Cd $(\text{ClO}_4)_2$ 0.01 M solution. The passivation process was monitored by luminescence spectroscopy in the 450–700 nm region, because the end point of the Cd^{2+} addition corresponds to that at which the intensity of the near band gap emission reaches a maximum.^{28,32} For the scattering measurements some suspensions were concentrated under vacuum without flocculation.

The suspensions were characterized by UV-visible absorption spectroscopy (Perkin-Elmer Lambda 6 spectrophotometer) and by transmission electron microscopy (Carl Zeiss TEM 902–80 keV). Sample preparation for the TEM measurements was done by placing a drop of the suspension onto a carbon/parlodium film supported on Cu grids and allowing it to dry under air at room temperature. Image processing (Scion Image) was performed in order to enhance the morphological information on the nanoparticles. The luminescence spectra of the CdS suspensions were obtained on a Jobin-Yvon Ramanor U-1000 spectrometer (1m monochromator, 150 W Xe lamp) at room temperature.

2.2. Hyper-Rayleigh Scattering Measurements. The values of the first hyperpolarizability β were determined from HRS measurements. The HRS method provides an unique technique for β measurements of nondipolar samples, which are out of reach of the standard electric-field-induced second harmonic (EFISH) generation technique. As known,³³ the HRS arises from an instantaneous anisotropy that breaks the centrosymmetry present in an otherwise homogeneous solution. The second harmonic signal in our experiments was created inside a glass cell with samples using the 10 ns, up to 30 mJ pulses at 1064 nm generated by a Q-switched Nd:YAG laser. After filtering out any residual flash lamp light with a high-pass filter, the fundamental light was collimated by two lenses to form a

parallel beam into the glass cell. The use of the collimated beam with a beam radius of 1.0 mm avoided solution dielectric breakdown and ensured an improved signal/noise ratio. The light scattered at a right angle to the incident beam was collected by a system of lenses and was measured by a photomultiplier tube with a low pass filter to suppress the fundamental light. In the high optical power densities used in HRS experiments, a fluorescence signal because of multiphoton excitation may also be present together with the HRS signal at the second harmonic wavelength.^{34–36} To verify the presence of fluorescence, we used a monochromator. A gated detection electronic was used for data acquisition. Each data point is the average of 1000 laser shots. Data were gathered for about 20 MW/cm² pulse energy. The samples were filtered through a 0.45 μm Teflon filter prior to the measurements in order to remove most microscopic particles which could otherwise induce breakdowns in the presence of the laser beam. The measurement error is expected to be about 5%.

To correctly analyze the experimental data, we should include three effects (viz. luminescence induced by multiphoton excitation, absorption at the fundamental frequency, and absorption at its first harmonic) in the formula describing the intensity of the light scattered at the second harmonic wavelength ($I_{2\omega}$) by an ensemble of species (molecules or particles) in a solvent:

$$I_{2\omega} = B\{N\langle\beta^2\rangle + N_{\text{sol}}\langle\beta_{\text{sol}}^2\rangle + N\Phi\}I_{\omega}^2 \left[\frac{1 - \exp[-2\alpha(\omega)L_1]}{2\alpha(\omega)} \right] \exp[-\alpha(2\omega)L_2] \quad (2)$$

where B is a constant depending on the experiment's geometry and local-field factors, N and $\langle\beta^2\rangle$ are the concentration and the orientation averaged first hyperpolarizability of the studied species, N_{sol} and $\langle\beta_{\text{sol}}^2\rangle$ are the corresponding values for the solvent, Φ is the luminescence quantum yield (we assume that the luminescence intensity depends linearly on the concentration³⁷), I_{ω} is the intensity of incident light with fundamental frequency, $\alpha(\omega)$ and $\alpha(2\omega)$ are the absorption coefficients at the fundamental frequency and at the double frequency, L_1 is the length of the scattered volume along the fundamental beam direction which is used by our collection system ($L_1 = 1$ cm), and L_2 is the propagation length for scattered light ($L_2 = 0.2$ cm). The term $[1 - \exp[-2\alpha(\omega)L_1]/2\alpha(\omega)]$ in (2) describes the effective scattered volume which is due to the absorption of the fundamental wave. In our case, the absorption at the fundamental frequency is negligible, as it can be easily deduced from the absorption spectra (besides, the absorption coefficient for CdS bulk at 1060 nm, including nonlinear effects, is only 0.035 cm/MW³⁸). Therefore, we corrected our results only for the absorption of the double frequency wave. The absorption coefficients $\alpha(2\omega)$ were determined from the linear absorption spectra of the samples. To determine the role of up-conversion luminescence we measured the emission spectra near double frequency upon excitation at 1064 nm.

The values of $\langle\beta^2\rangle^{1/2}$ were determined from the intensity of the doubled frequency light $I_{2\omega}$ by the internal reference method.^{39–41} In this method, the β value was determined from (2) using the intensity $I_{2\omega}$ measured for suspensions containing different concentrations N of CdS nanocrystals. The $\langle\beta^2\rangle^{1/2}$ values were taken to be 0.56×10^{-30} esu for water molecules.⁴² For comparison, the values of $\langle\beta^2\rangle$ for some samples were also determined by the external reference method^{40,41} using solutions

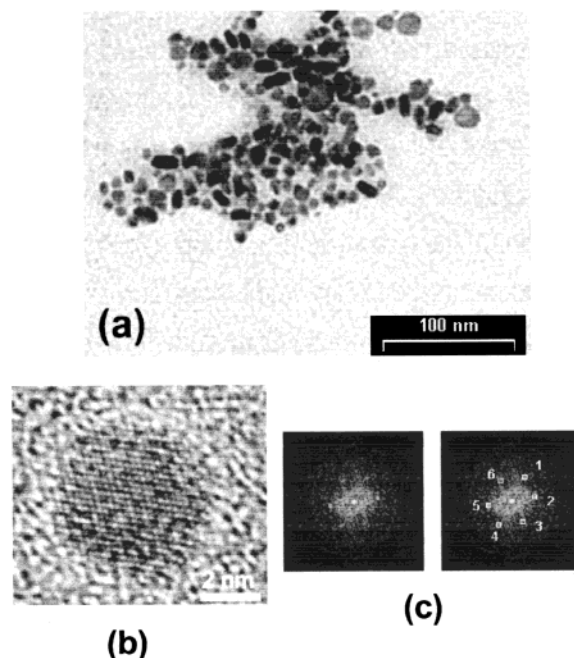


Figure 1. (a) TEM image of CdS nanoparticles from an aqueous suspension (Cd/S ratio = 1.0), (b) HRTEM image for a single CdS nanoparticle, and (c) selected area electron diffraction pattern from a CdS nanoparticle.

of para-nitroaniline in methanol as a reference sample. The β values obtained by the two methods are in good agreement with each other.

In the external method, the intensity $I_{2\omega}$ scattered from the studied sample is compared with the intensity of the second-harmonic light scattered from a reference sample $I_{\text{ref}2\omega}$:

$$\frac{I_{2\omega}}{I_{\text{ref}2\omega}} = \frac{N\langle\beta^2\rangle^{1/2} + N_{\text{sol}}\langle\beta_{\text{sol}}^2\rangle^{1/2}}{N_{\text{ref}}\langle\beta_{\text{ref}}^2\rangle^{1/2} + N_{\text{ref,sol}}\langle\beta_{\text{ref,sol}}^2\rangle^{1/2}} \quad (3)$$

where the terms $\langle\beta_{\text{ref}}^2\rangle$, $\langle\beta_{\text{sol}}^2\rangle$, and $\langle\beta_{\text{ref,sol}}^2\rangle$ are the average first hyperpolarizabilities of the reference material, the solvent of the investigated sample (water), and the solvent of the reference substance (methanol), respectively, and N_{ref} , N_{sol} , and $N_{\text{ref,sol}}$ are the corresponding concentrations. The reference substance was para-nitroaniline dissolved into methanol at a concentration of 10^{20} molecules cm⁻³. We assumed that despite the different point symmetries of the species probed by measurements, the main contribution into $\langle\beta^2\rangle$ is due to the component β_{ZZZ} , and $\beta_{\text{ZZZ}} = (35/6)^{1/2} \langle\beta^2\rangle^{1/2}$.^{40,41} The β_{ZZZ} values were taken to be 0.69×10^{-30} esu for methanol⁴⁰ and 34.5×10^{-30} esu for para-nitroaniline.³⁹ The local field factors were assumed identical between the different solvents.

3. Results and Discussion

3.1. Band-Gap Dependence of the First Hyperpolarizability. A TEM image of the CdS nanoparticles obtained from sample 3 (Cd/S ratio= 1.0) is shown in Figure 1a. The mean particle diameter is estimated to be 9.0 nm. Figure 1b presents the HRTEM image of a single CdS nanoparticle, as a representative example. It can be observed that the nanoparticles are well crystallized, with interplanar distances of 2.6 Å, which is in good agreement with the Cd–S bond length in both the zinc blende and the wurtzite CdS crystal structures (2.52 and 2.53 Å, respectively³⁸). The selected area electron diffraction pattern (Figure 1c) is also inconclusive with respect to the crystal

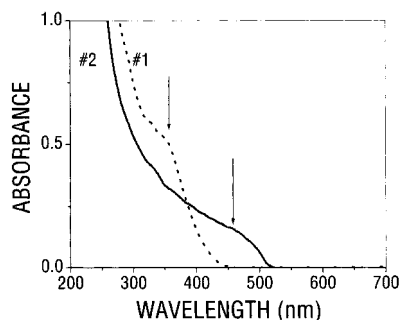


Figure 2. Absorption spectra of two of the investigated samples of colloidal suspensions of CdS nanocrystals (sample 1, dots; sample 2, solid line). The arrows indicate the wavelength where the first derivative is zero and second derivative is positive.

structure, because it yields only one lattice plane distance (viz 2.0 Å), which can be ascribed either to the (220) planes of cubic zinc blende CdS ($d = 2.06$ Å) or to the (110) planes of hexagonal wurtzite CdS ($d = 2.07$ Å). However, the powder X-ray diffraction patterns of the dried suspensions can be unambiguously indexed to the zinc blende crystal structure of CdS. The diffraction peaks are broadened because of the finite size of the particles, allowing the average nanocrystal size to be estimated by using the well-known Scherrer's formula. The sizes estimated from the X-ray diffraction peaks are in good agreement (i.e., $\pm 10\%$) with those derived from the TEM measurements.

The mean sizes of nanocrystalline CdS particles can also be estimated from the UV–visible absorption spectra,⁴³ by using the well-established relationship between the nanoparticle size and the excitonic transition energy (i.e., the wavelength where the first absorption maximum occurs), provided that the particles are in the quantum size confinement regime.^{1–3,10,13,43} Considering the aim of this work, UV–visible absorption spectroscopy is a much more convenient technique to estimate the mean sizes of CdS nanocrystals in colloidal suspensions, provided the particles are within the quantum size confinement regime. Furthermore, it has the important advantages of probing the whole sample used for the HRS measurements and allowing the analysis of the samples as-prepared and after the measurements.

Figure 2 shows the UV–vis absorption spectra for two of the aqueous colloidal suspensions of polyphosphate stabilized CdS nanocrystals investigated (sample 1 with Cd/S ratio = 4.0 and sample 2 with Cd/S = 1.6). The wavelengths corresponding to the absorption maxima were found from the second derivative of the spectra. The mean particle diameters are thus estimated to be 2.0 nm for sample 1 and 5.6 nm for sample 2. The particle diameter for sample 3 (Cd/S = 1.0) was determined to be 9 nm, in very good agreement with the sizes determined by TEM and powder X-ray diffraction (8.9 ± 1.6 and 9.9 nm, respectively). These results show that the mean particle size decreases if the Cd/S ratio increases, while keeping all other variables constant. The formation of CdS particles in aqueous solution involves two steps:³¹ (a) seed formation by reaction between free Cd^{2+} and S^{2-} ions and (b) growth of the seeds, either by Ostwald ripening or by reaction between Cd^{2+} and S^{2-} ions released from chemical equilibria. The average particle size will thus be determined by the pH before H_2S injection and the duration of ripening after the precipitation.^{28–31,43} In the present case, the precipitation at pH 8.5 leads to rapid seed formation and slow Ostwald ripening.^{28,31} The excess of Cd^{2+} will hinder further seed growth by both mechanisms.³¹

The results presented above are consistent with the well-established observation that room-temperature synthesis of CdS

TABLE 1: Composition of the $\text{Cd}_x\text{Zn}_{1-x}\text{S}$ Nanocrystals and the Values Obtained for the First Hyperpolarizability $\langle \beta^2 \rangle^{1/2a}$

x	$\langle \beta^2 \rangle^{1/2}$, 10^{-27} esu	energy (E_g), eV	x	$\langle \beta^2 \rangle^{1/2}$, 10^{-27} esu	energy (E_g), eV
1	63.4	2.57	0.75	9.7	3.31
0.25	14.9	2.86	0	6.6	3.79

^a The mean particle diameter D is 9 nm, and the concentration N is $1.8 \times 10^{14} \text{cm}^{-3}$ for all samples.

nanocrystals yields the zinc blende structure.^{3,31,43,44} The thermodynamically favored wurtzite crystal structure is typical for macrocrystalline CdS and is obtained only when high temperatures are used during the preparation.^{31,43} This shows that at room temperature the particles are grown under kinetic control.⁴³ Under these conditions, the particle sizes will be solely determined by the physical–chemical variables during the growth (i.e., pH, temperature, metal ion and S^{2-} concentrations, and metal/sulfur ratio^{28,29,31,43,44}). It has previously been shown²⁸ that the simultaneous precipitation of ZnS and CdS leads to a co-colloid, whose absorption onset is continuously blue shifted with increasing Zn content, implying that $\text{Cd}_x\text{Zn}_{1-x}\text{S}$ particles are formed, because a mixture of pure CdS and ZnS particles could not give rise to band-gaps intermediate to those of ZnS and CdS. Considering that ZnS and CdS are isostructural and have a small lattice mismatch (7%),³⁸ it can be expected that the crystal structure and particle sizes of the $\text{Cd}_x\text{Zn}_{1-x}\text{S}$ nanocrystals will be independent of the $\text{Cd}^{2+}/\text{Zn}^{2+}$ ratios, provided that the total M^{2+} concentration ($\text{M} = \text{Cd}$ and/or Zn) and all other variables (viz. pH, M/S ratio, temperature, etc.) are kept constant. This is specially reinforced at pH 8.5, which leads to fast seed formation^{29,31} and thus stricter kinetic control.

To establish the band-gap dependence of the first hyperpolarizability β , we performed HRS measurements for four colloidal suspensions of polyphosphate stabilized $\text{Cd}_x\text{Zn}_{1-x}\text{S}$ nanocrystals of the same mean diameter (9 nm) but with different composition. Figure 3 presents TEM images and size histograms for three of the investigated $\text{Cd}_x\text{Zn}_{1-x}\text{S}$ samples ($x = 1, 0.25$, and 0). The histograms were obtained from the analysis of 500–600 nanoparticles. It can be concluded that the mean particle size is 9 nm for all of the $\text{Cd}_x\text{Zn}_{1-x}\text{S}$ suspensions investigated in this work, as expected considering that the conditions during the synthesis were thoroughly controlled and were the same in all preparations. The standard deviation of the size distribution is comparable for all samples ($\sim 20\%$) and is consistent with the values reported in the literature for similar synthetic methods ($\sim 15\%$ ^{28–32}). The results from powder X-ray diffraction confirm that the particle sizes and the crystal structure are not a function of the Zn/Cd ratio.

Figure 4a shows the UV–vis absorption spectra of the investigated samples. A blue shift of the absorption edge with increasing Zn^{2+} concentration is easily observed. From the first absorption maxima in the spectra, we obtained the band-gap energies E_g for all four compositions. The observed shift in the band-gap energy with the (Zn, Cd)S nanoparticle composition agrees well with the trend expected based on the literature data for bulk (Zn, Cd)S alloys^{45b} (Figure 4b). This provides strong evidence that the Cd:Zn ratio in the solution is indeed maintained in the (Zn, Cd)S nanoparticles, as expected considering that the coprecipitation is quantitative and very fast (K_{ps} values are 1×10^{-28} and 4×10^{-24} for CdS and ZnS respectively). The powder X-ray diffraction patterns of the dried suspensions are also consistent with the expected composition of the (Zn, Cd)S nanoparticles. The results above show that the main effect of the alloy composition change is the band-gap shift (i.e., sizes,

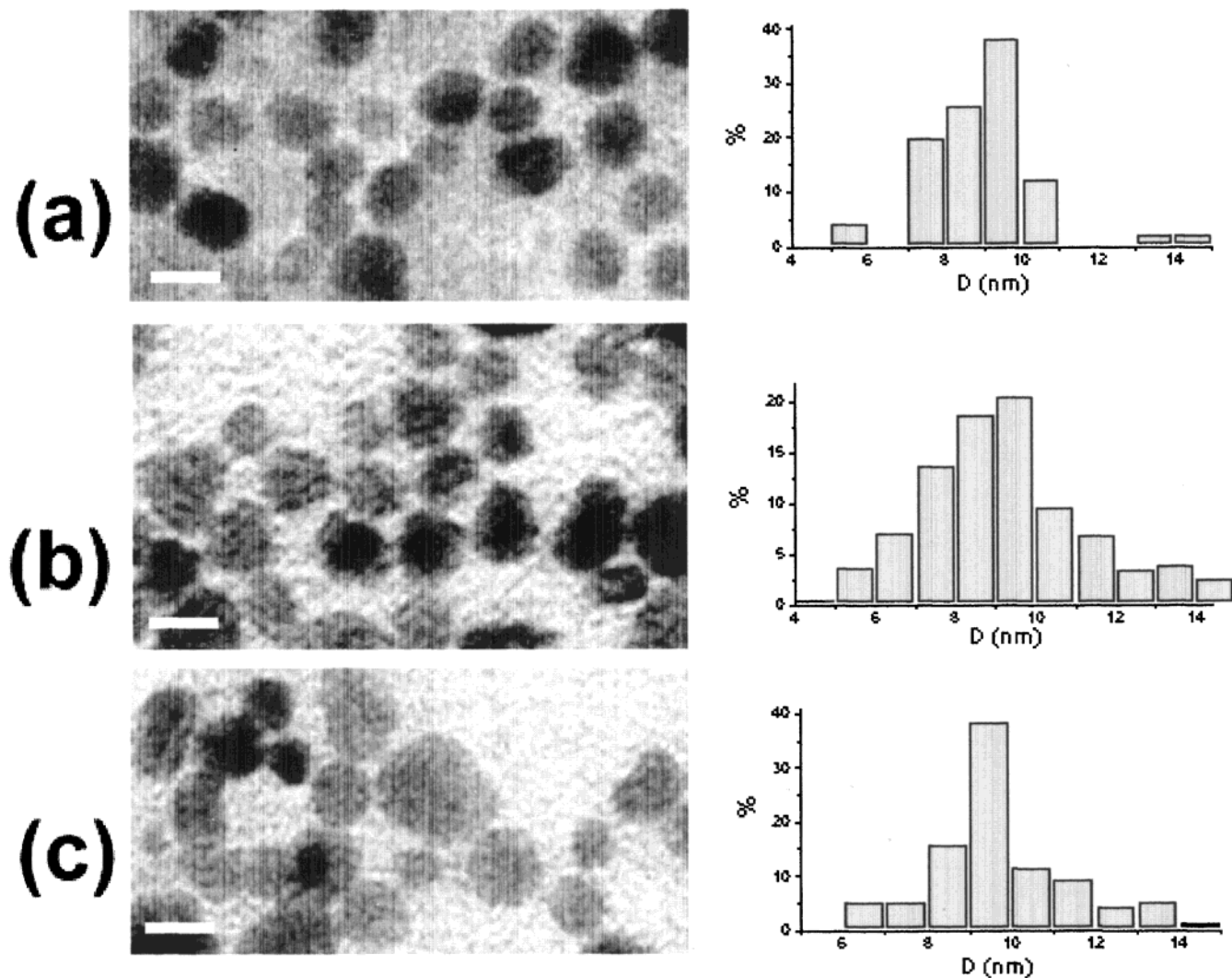


Figure 3. TEM images and size distribution histograms (500–600 particles) for $\text{Cd}_x\text{Zn}_{1-x}\text{S}$ nanocrystals for $x = 1$ (a), 0.25 (b), and 0 (c).

crystal structure, and surfaces of the nanoparticles are not observably affected).

The concentration of $\text{Cd}_x\text{Zn}_{1-x}\text{S}$ nanocrystals in the suspensions was estimated from the known $\text{Cd}_x\text{Zn}_{1-x}\text{S}$ concentration and mean particle sizes, assuming that the precipitation is quantitative and that the nanocrystals developed the zinc blend crystal structure (unit cell parameters: $Z = 4$; $a_0 = 0.5410$ nm for ZnS and 0.5825 nm for CdS,³⁸ and a linear variation for $\text{Cd}_x\text{Zn}_{1-x}\text{S}$ depending on x), as argued above.^{31,43,44} The $\langle\beta^2\rangle^{1/2}$ values determined for the four samples are presented in the Table 1. Figure 5 shows the experimental values of $\langle\beta^2\rangle^{1/2}$ versus the band-gap energy E_g (points), as well as a best fitting curve obtained using (4), which will be discussed below. It is important to notice that the absorption spectra remains unchanged after the HRS measurements, showing that the particle concentration and particle sizes were not affected by photoetching, dielectric breakdown, or clustering and destabilization of the colloidal suspension.

Considering that ZnS and CdS are direct band gap semiconductors and that the valence and conduction bands are formed, respectively, from the S^{2-} 3p states and the 5s (or 4s) states of Cd^{2+} (or Zn^{2+}),³⁸ the band gap optical transition in $\text{Cd}_x\text{Zn}_{1-x}\text{S}$ can be seen in first approximation as a ligand to metal charge-transfer excitation. Therefore, a two-level model proposed in ref 46 can be applied to explain the observed dependence of β on the energy gap E_g between the fundamental and the first

excited states:

$$\beta = \frac{3e^2\hbar^2 E_g \Delta\mu}{2m(E_g^2 - E_0^2)[E_g^2 - (2E_0)^2]} \quad (4)$$

Here m and e are the electron's mass and charge, respectively, E_0 is the energy of incident photons, f is the transition oscillator strength, and $\Delta\mu$ is the change in the dipole moment between the ground and excited states. The curve in Figure 5 was fitted assuming that f and $\Delta\mu$ do not depend on the alloy composition. Although this is a rough assumption because it can be expected that $\Delta\mu$ and f will be different for CdS and ZnS because of the different M–S bond polarizabilities, the good correspondence between the experimental data points and the fitting curve shows that the band-gap energy E_g is the most relevant variable in the present case. The decrease of β with decreasing x in the $\text{Cd}_x\text{Zn}_{1-x}\text{S}$ nanocrystals can thus be ascribed to the decrease of the relative resonance enhancement, because the energy difference between E_g and E_0 increases. As will become clear below, this implies that quantum size effects do not play an important role for 9 nm $\text{Cd}_x\text{Zn}_{1-x}\text{S}$ nanocrystals.

As the size of a semiconductor cluster increases, it is possible to distinguish several size regimes in the development of its properties, which progressively change until the bulk values are reached.^{2,10} Very small clusters (up to a few tens of atoms) have

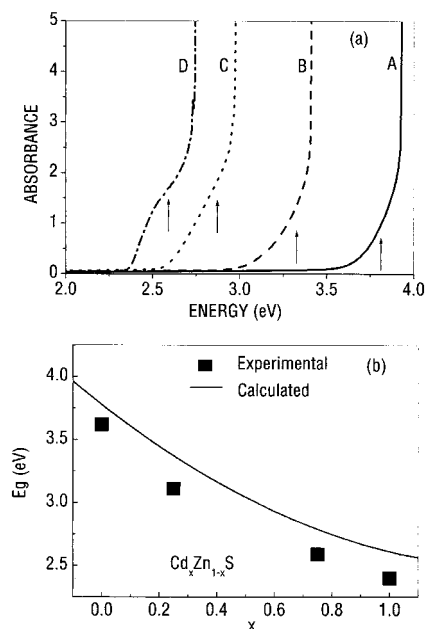


Figure 4. (a) Absorption spectra for the investigated samples of colloidal suspensions of $\text{Cd}_x\text{Zn}_{1-x}\text{S}$ nanocrystals for $x = 0$ (A), 0.25 (B), 0.75 (C), and 1 (D). The arrows indicate the energy where the first derivative is zero and second derivative is positive. (b) Band-gap energy as a function of the alloy composition for $\text{Cd}_x\text{Zn}_{1-x}\text{S}$ nanoparticles (circles; this work) and bulk (squares; ref 45b). The values of x for the nanoparticles refer to the nominal concentration in the solution prior to the coprecipitation. The band-gap values for the bulk were calculated from the empirical relation $E_g = E_{g(\text{ZnS})} - 1.78x + 0.61x^2$.^{45b}

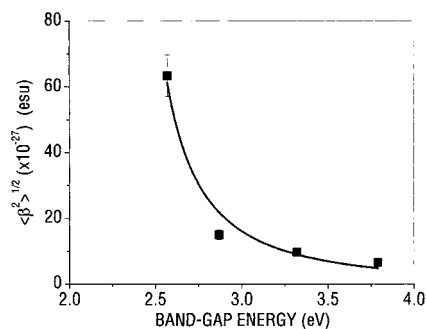


Figure 5. First hyperpolarizability $\langle \beta^2 \rangle^{1/2}$ as a function of the band-gap energy for the investigated samples of colloidal suspensions of $\text{Cd}_x\text{Zn}_{1-x}\text{S}$ nanocrystals. The points are experimental data, whereas the solid line is the best-fitting curve following eq 4.

an essentially molecular behavior. Larger clusters, but with a radius R smaller than both the electron and the hole Bohr radii (a_e and a_h , respectively) are in the so-called strong confinement regime, in which both the electron and hole are confined, with minor electron–hole correlation.^{2,10} In the weak confinement regime, $a_e, a_h < R \leq \sim 2 - 4a_0$ (a_0 is the exciton Bohr radius) and only the hydrogenic exciton is confined. An intermediate regime (moderate confinement) can be recognized when only one of the charge carriers (viz. the electron, because the hole is heavier) is confined (i.e., $a_h < R \leq a_e$). The values of a_0 , a_e , and a_h are determined by the high-frequency dielectric constant ϵ_∞ and the electron and hole effective masses (m_e and m_h , respectively) in the semiconductor.¹³ For zinc blende ZnS ($E_g = 3.7$ eV; $\epsilon_\infty = 5.4$; $m_e = 0.34m_0$; and $m_h = 0.5m_0$)³⁸ a_0 , a_e , and a_h are thus 1.5, 0.84, and 0.57 nm, respectively, whereas for zinc blende CdS ($E_g = 2.5$ eV; $\epsilon_\infty = 5.3$; $m_e = 0.14m_0$; and $m_h = 0.51m_0$)³⁸, these values are 2.6, 2.0, and 0.55 nm, respectively. For $\text{Cd}_x\text{Zn}_{1-x}\text{S}$ particles, the values of a_0 , a_e , and a_h will vary from the ZnS to the CdS values as the x increases.

Therefore, for a given size, the magnitude of the quantum size effects for $\text{Cd}_x\text{Zn}_{1-x}\text{S}$ particles can be expected to increase with x . However, this is not observed in our experiments because for 9 nm $\text{Cd}_x\text{Zn}_{1-x}\text{S}$ particles the weak confinement regime is realized throughout the composition range investigated, thus allowing the band gap dependence to be clearly evidenced.

3.2. Surface Effects. Considering that a large percentage of the atoms in a nanoparticle is on or near the surfaces (e.g., for a 5 nm CdS particle, $\sim 15\%$ of the atoms are on the surface), one could expect a profound effect of the surface and its surroundings on the particle properties.¹³ However, these surface effects have been shown to be restricted to some properties, such as charge carrier dynamics,^{47,48} photodarkening,⁴⁷ photochemical activity,^{29,31,48} and photoluminescence quantum yields,^{3,29,31,32,48} whereas the band gap, the absorption oscillator strengths, and the spectral hole width were found to be unaffected by the particle surface.⁴⁸

The nonlinear optical response of a particle will have both bulk and surface contributions.⁵³ For nanoparticles of noncentrosymmetric material (such as zinc blende CdS or ZnS, space group symmetry: $F - 43m^{38}$) the bulk contribution can be expected to dominate over the surface contribution,⁵³ which should be important for centrosymmetric materials^{22,53} and metallic particles.^{49,53} It must be realized that in a transparent noncentrosymmetric material the nonlinear optical signal is generated in a layer about $1/4\lambda$ thick,⁵⁴ so that for a nanoparticle, the SHG signal will not be surface specific, because the surface and the bulk contributions will be detected together and may not be separable from each other.⁵³ Further, the interfacial layer may be as thick as several tens of monolayers.⁵³ Nevertheless, the magnitude of the surface contribution can be effectively deduced by perturbing the surface and then evaluating the effects on the nonlinear optical response.⁵³

The influence of the surface capping agent [viz. AOT⁻, i.e., Ibis (2-ethylhexyl) sulfosuccinate, pyridine, or SC(NH₂)₂] or surface termination (S²⁻ rich or Cd²⁺ rich) on the first hyperpolarizability β of CdS nanocrystals in organic solvents or water was investigated by Lu et al.^{22–24} The β values were observed to be different for CdS nanocrystals with different surfaces, but the differences were not very large ($\sim 30\%$). The influence of the surface stabilizer (viz. PVP, poly(vinylpyrrolidone); ME, mercaptoethanol; MPA, mercaptopropionic acid; or LC: L-cysteine) on the relative magnitude of the SHG signal by colloidal aqueous suspensions of CdS nanocrystals was also investigated by Brysch et al.²⁵ The SHG signal was observed to increase by a factor 2 from PVP to ME, by a factor 3 from PVP to LC and by an order of magnitude from PVP to MPA as the stabilizers.²⁵

It must be realized, however, that refs 22–25 overlooked the fact that by changing the stabilizer one might also induce changes in the particle sizes and size distributions^{31,43} or even in the crystal structure.⁴³ Further, no attempt was made to take into account the contribution of the stabilizer itself to the HRS signal. Because most stabilizers are organic molecules or polymeric chains their possible contribution is most likely not negligible.

Therefore, to unambiguously evaluate the relative contribution of the surface, we measured the β values for the same ensemble of 9 nm polyphosphate stabilized CdS nanocrystals, prior to and after their surface modification with OH⁻. In this way, the size and the stabilizer of the particles are kept unchanged, only the surface being modified. Figure 6a shows the absorption spectra of the investigated CdS suspension prior to and after the surface modification. The position of the minimum of the

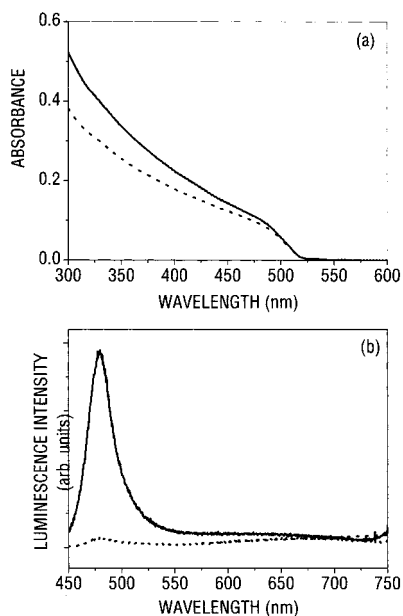


Figure 6. (a) Absorption spectra and (b) luminescence spectra excited at 365 nm for the investigated sample of colloidal suspension of CdS nanocrystals prior to (dots) and after (solid line) surface passivation by OH^- .

first derivative of the spectra is not affected by the modification, what shows that the mean diameter of the CdS core remains the same, as indeed expected. The increase observed in the nanoparticles absorption after modification can be ascribed to the absorption by the $\text{Cd}(\text{OH})_2$ layer. The formation of $\text{Cd}(\text{OH})_2$ particles and coalescence of CdS particles can be ruled out because this would increase Mie scattering, thus increasing the spectral background. The HRS signal was observed to increase by a factor 2.8 after the surface modification, what means that the value of β was enhanced by a factor 1.7. A possible explanation for this enhancement will be discussed below.

The luminescence of OH^- passivated CdS suspensions is ~ 20 times more intense than that of the original suspensions (Figure 6b) and consists of a rather narrow and strong band around 480 nm. The weak broad emission band of the CdS suspensions prior to the OH^- passivation are ascribed to the radiative recombination of photogenerated charge carriers in deep traps of different energy depths (deep trap luminescence).²⁹ These traps are associated with surface defects, such as sulfur vacancies^{29,31} or HS^- radicals.^{29,31} The low quantum yield of this emission (viz. $\leq 1\%$) is an indication that the radiationless recombination is the dominating process.^{29,31,32} The blue-green luminescence observed after the OH^- surface modification is attributed to electron trapping in very shallow traps (≤ 0.1 eV),^{29,31} followed by radiative recombination of the charge carriers either during the trapping (near band gap luminescence) or after thermal detrapping (band edge luminescence).^{29,31} This mechanism is corroborated by the longer lifetimes observed after the passivation.³² The higher quantum yields observed after passivation (viz. $\geq 10\text{--}50\%$) can be ascribed to lower radiationless decay rates, because of a lower concentration of surface states associated with deep traps.^{29,32}

The surface of polyphosphate (PP) stabilized CdS nanocrystals in colloidal water suspensions has been shown to be mostly Cd^{2+} terminated.³ The negatively charged PP chains are bound to the surface Cd^{2+} cations through their oxygens, thus preventing particle agglomeration and coalescence by both electrostatic and sterical repulsions.³¹ The modification of the

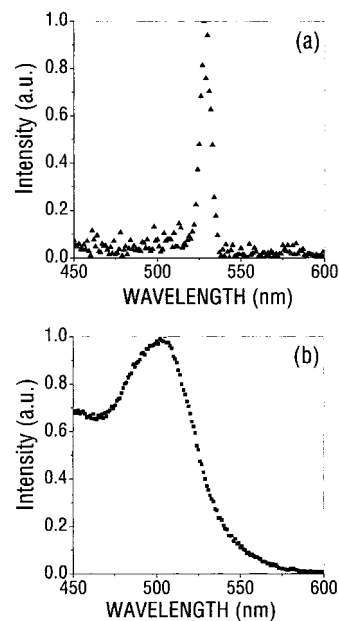


Figure 7. Spectra (luminescence plus scattered light) of a colloidal suspension of CdS nanocrystals (sample #3) upon laser excitation at 1064 (a) and 355 nm (b), recorded by using the HRS setup.

TABLE 2: Concentration of CdS Nanocrystals N and the Mean Particle Diameter D for the Samples Investigated, the Values Obtained for the First Hyperpolarizability $\langle\beta^2\rangle^{1/2}$, and the First Hyperpolarizability Normalized Per CdS Pair $\langle\beta^2\rangle^{1/2}/N_{\text{CdS}}$

sample	N cm^{-3}	D nm	$\langle\beta^2\rangle^{1/2}$, 10^{-30} esu	N_{CdS}	$\langle\beta^2\rangle^{1/2}/N_{\text{CdS}}$, 10^{-30} esu
1	1.7×10^{15}	2	2.1	85	24.7
2	7.9×10^{13}	6	21.4	1865	11.5
3	1.8×10^{13}	9	76.4	8002	9.5

surface of the CdS nanocrystals consists of two steps. In the first step, the high pH induces the precipitation of a $\text{Cd}(\text{OH})_2$ layer on the surface and converts SH^- groups to S^{2-} .²⁹ In the second step, the added Cd^{2+} ions bind to surface S^{2-} and OH^- ions, forming a predominantly Cd^{2+} terminated surface, which is required to keep the stabilization by the PP^{n-} anions. We can thus propose that the passivation by OH^- changes the nature of the surface terminating groups from $\text{S}^{2-}-\text{Cd}^{2+}-\text{PP}^{n-}$, $\text{S}^{2-}-\text{Cd}^{2+}-\text{S}^{2-}$, and $\text{S}^{2-}-\text{Cd}^{2+}-\text{SH}^-$ ²⁹ to $\text{S}^{2-}-\text{Cd}^{2+}-\text{OH}^-$ ²⁹ and $\text{S}^{2-}-\text{Cd}^{2+}-\text{OH}^- - \text{Cd}^{2+}-\text{PP}^{n-}$, thus removing deep trap states. Further, because $\text{Cd}(\text{OH})_2$ has a much wider band gap than CdS, the charge carriers will be mostly confined into the bulk of the particle where the defect concentration is lower. The luminescence results discussed above corroborate these assumptions. The enhancement of the first hyperpolarizability β after the surface modification can thus be ascribed to a larger surface electric dipole, because of the much more asymmetric structure of the surface terminating bonds after the passivation.

3.3. Size Dependence of the First Hyperpolarizability.

Finally, we turn to the size dependence of β . The HRS measurements were performed in three samples of colloidal suspensions of polyphosphate stabilized CdS nanocrystals with different mean sizes. The UV-vis absorption spectra for two of these samples have been shown above (Figure 2). The results obtained, the concentration of CdS particles N , and the mean particle diameter D for the samples studied are shown in Table 2. The method employed to determine the mean diameters D and the concentration of the particles N , as well as aspects concerning the structure and preparation of the nanocrystals, have been discussed in section 3.1. We point out that the

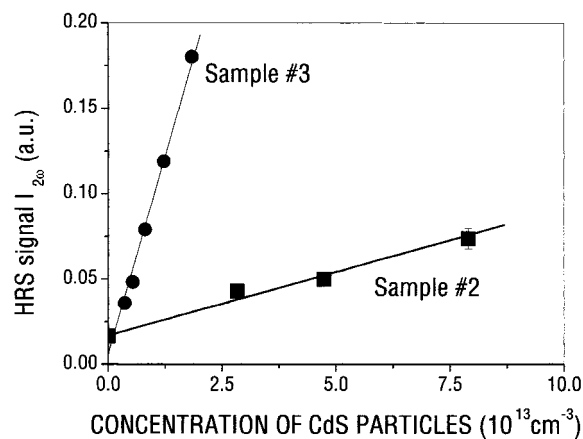


Figure 8. Intensity of the scattered second harmonic light for varying concentration of CdS nanocrystals for samples 2 and 3. The solid lines are the best fitting curves.

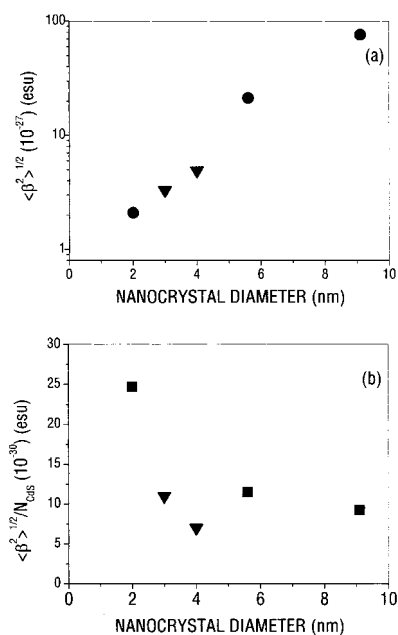


Figure 9. First hyperpolarizability $\langle \beta^2 \rangle^{1/2}$ (a) obtained by the internal method (circles), and its value normalized per single CdS pair ($\langle \beta^2 \rangle^{1/2} / N_{\text{CdS}}$) (b) as a function of the CdS nanocrystal diameter. Data from ref 22 are also included (down triangles).

difference between the β values for CdS nanocrystals of the same mean size presented in Tables 1 and 2 provides a good illustration of the overall experimental accuracy and reproducibility (i.e., measurement plus sample preparation).

To evaluate the possible contribution of multiphoton excited luminescence to the total signal at 532 nm, the scattered light from the sample was dispersed through a monochromator. Representative spectra for sample 3 (9 nm), obtained under excitation at 1064 and 355 nm, are shown in Figure 7. One can easily conclude that the intensity of multiphoton excited luminescence is negligible, and therefore, the signal measured at 532 nm can be totally ascribed to the HRS process.

Figure 8 shows the intensity of HRS signal versus the concentration of CdS nanocrystals for samples 2 and 3. The $\langle \beta^2 \rangle^{1/2}$ values obtained for these samples using the internal reference method are given in Table 2. The observed β values are among the largest observed for solution samples. In Figure 9a, we present the $\langle \beta^2 \rangle^{1/2}$ values versus the mean diameter of the CdS nanocrystals. Data from ref 22 are also included for comparison (down triangles). It must be emphasized that data

from ref 22 concerns AOT⁻ stabilized CdS nanocrystals in organic solvents, whereas our data was obtained from PP⁻ stabilized CdS nanocrystals in water. The consistency observed between data obtained for particles prepared by different techniques, with different stabilizers and suspended in different media, shows that the bulk contribution is indeed the dominating one, as pointed out in the previous section.

The bulk contribution is due to the noncentrosymmetric nature of the CdS zinc blende crystal structure and, therefore, arises from the polarizability of the individual Cd – S bonds. The increase of β with the diameter of the CdS nanocrystal (Figure 9a) is thus obviously due to the growing amount of the second harmonic generating material. To correct the data for this volume dependence, the β values were normalized per CdS pair (β / N_{CdS} , hereafter dubbed β_{CdS}), where N_{CdS} is the number of CdS pairs per particle (N_{CdS} can be estimated from the known particle volume and the lattice parameters of zinc blende CdS³⁸). This normalization procedure shows that, although β increases with the particle size (Figure 9a), β_{CdS} increases with decreasing of the particle size (Figure 9b). A similar size dependence has been recently reported by Jacobsohn and Banin²⁷ for the first hyperpolarizability of CdSe nanocrystals.

The observed size dependence of β_{CdS} (and also β_{CdSe}) can be the result of the enhancement of both the bulk and the surface contributions. As we argued before,²⁶ the bulk contribution can be enhanced because of quantum confinement effects on the exciton oscillator strength. The volume normalized exciton oscillator strength and the exciton binding energy have been predicted to increase with decreasing particle size for $R < a_0$ (a $1/R^3$ dependence), because of the enhanced spatial overlap between the electron and hole wave functions and the coherent motion of the exciton.^{13,51} This size dependence of the normalized exciton oscillator strength has been experimentally confirmed for CdS nanocrystals by two independent groups,^{43,52} although not in complete agreement with the theoretical dependence. Van Dijken et al.⁵² reported an increase by a factor of 3.5 for a radius reduction from 2.4 to 1.1 nm, whereas Vossmeier et al.⁴³ observed no clear effect from 4.8 to 2.8 nm, an increase by a factor of ~ 4 from 2.8 to 1.2 nm and a good agreement with theory (i.e., a $1261/R^3$ dependence) for smaller radii (1.2 to 0.64 nm). As can be readily observed in (4), an increase in the oscillator strength f will increase β . Furthermore, the change in the dipole moment between ground and excited states $\Delta\mu$ is proportional to f , thus also contributing to the enhancement of β . The fact that the enhancement observed in β_{CdS} (a factor of 2.6 from 9 to 2 nm) is smaller than the increase in f reported in refs 43 and 52 can be ascribed to the counteracting effect of the band-gap E_g , which increases with the decrease of size, thus reducing β , as demonstrated above (section 3.1).

Because the surface-to-bulk ratio increases with the reduction of size, surface effects could also contribute to the observed enhancement of β_{CdS} . In ref 27, surface effects (viz. the highly noncentrosymmetric electron distribution around surface atoms specially in nonspherical shapes, the surface polarization instability of the electron and hole in the quantum dots,⁵³ and the highly polarizable dangling bonds because of imperfect surface passivation) were assumed to be the only plausible explanation for the size dependence reported for CdSe nanocrystals. Quantum size effects were assumed to play no role. However, the fact that the enhancement observed for the CdSe nanocrystals is larger (a factor 5)²⁷ than the enhancement reported here for CdS nanocrystals in same size range, provides strong evidence that neglecting the above-mentioned quantum

size effects is not justified. For wurtzite CdSe ($E_g = 1.8$ eV; $\epsilon_\infty = 5.8$; $m_e = 0.13m_0$; and $m_h = 0.45m_0$ ³⁸), a_0 , a_e , and a_h are 3.5, 2.4, and 0.7 nm, respectively, whereas for zinc blende CdS (see above), a_0 , a_e , and a_h are 2.6, 2.0, and 0.55 nm, respectively. Therefore, the quantum size effects can be expected to be more pronounced for CdSe than for CdS in the same size range.

Furthermore, when ascribing the observed enhancement in the volume normalized β to the increase in the surface/bulk ratio, one implicitly makes the assumption that either β_{surface}/N is inherently larger than β_{bulk}/N (N being the number of cation–anion pairs), which is not necessarily true (see section 3.2), and/or that β_{surface}/N is also size dependent. The latter possibility could be due to the surface polarization. Banyai et al.⁵³ have proposed that a semiconductor nanocrystal suspended in a dielectric medium experiences a surface polarization, which affects the electron–hole interaction, attracting them toward the surface, thus counteracting the effect of the quantum confinement potential.⁵³ The heavier hole is much more sensitive to this interplay of opposite effects, leading to a size dependent scenario, where the hole may be either cushioned away from the surface and pushed toward the center of the particle (volume exciton state) or trapped at the surface (surface exciton state), with the latter becoming more and more significant as the size of the quantum dot decreases, until a transition from volume to surface dominated exciton states occurs. We notice that the trapping of the hole at the surface while the electron is still delocalized increases the charge separation.⁵³ The surface field, if present, could induce additional nonlinearity.⁵⁴

Crystal structure effects can be ruled out because it is known that the crystal structure of polyphosphate stabilized CdS nanocrystals is independent of size.^{31,43} The shape of the nanocrystals, however, might be important. Although it is usually rather difficult to reliably determine the shape of nanoparticles, CdSe nanocrystals are known to be slightly prolate, with the aspect ratio being size dependent.²⁷ There are a few cases where the shape of CdS nanocrystals has been reported.^{3,25,43,44} Some authors have observed the particles to be faceted (truncated pyramids or tetrahedra)^{3,43} or prolate ellipsoids,^{43,44} whereas others have claimed the particles to be nearly spherical.²⁵ In this work, we have observed that the shape of the nanoparticles varies from nearly spherical to slightly prolate within one single sample. The extent to which this deviation from sphericity affects the HRS signal is not known and further work is required in order to clarify this matter.

The β value for bulk CdS can be roughly estimated to be 5×10^{-30} esu from the known value of the bulk nonlinear coefficient $d = 44$ pm/V⁵⁰ using [ref 8, pp 60–61]

$$\beta_{\text{bulk}} = \frac{N_g}{N_p} \frac{2\epsilon_0}{f(2\omega)f^2(\omega)} d \quad (5)$$

where N_p is the concentration of CdS pairs (in pairs/cm³), which can be calculated from the CdS density (4.82 g cm⁻³³⁸) and the CdS molar weight, N_g is the number of equivalent sites in the CdS unit cell (taken to be 1), and f is the local field factor. For optical local field factors, we used the expression in the Debye formalism appropriate for nonassociating liquids: $f(\omega) = (n(\omega)^2 + 2)/3$ [ref 50, page 248], where $n(\omega)$ is the refractive index. For optical fields factors, dispersion can be ignored, i.e., $n(\omega) = n(2\omega)$. The value obtained from eq 5 is the microscopic β , i.e., the first hyperpolarizability β per CdS pair, and it has therefore the same sense as the values of β/N_{CdS} shown in Figure 9b. The comparison shows that the value of β_{CdS} for 9 nm particles is twice as large as the bulk value. Because quantum

confinement effects are weak for this size (see section 3.1), the difference can be ascribed to surface effects. However, one should bear in mind that the polyphosphate stabilized CdS nanocrystals have the cubic zinc blende structure,^{3,31,43} whereas macrocrystalline CdS nearly always is hexagonal wurtzite,³¹ so that their values of β are not rigorously comparable. Nevertheless the difference between the microscopic β for the zinc blende and the wurtzite structures cannot be expected to be as large as a factor 2, because both structures are noncentrosymmetric (space groups: $F-43m$ and $P6_3mc$, respectively³⁸) and have the same Cd–S bond distance (0.252 nm³⁸).

4. Conclusions

The first hyperpolarizability β of 9 nm Cd_xZn_{1-x}S nanocrystals is observed to increase with x , what is attributed to the increase of the resonance enhancement because of the decrease of the band-gap energy. The modification of the surface of 9 nm CdS nanocrystals with OH⁻ enhances β by a factor of 1.7. This is ascribed to a larger surface electric dipole after the modification. Finally, the values of β of CdS nanocrystals are observed to increase with the particle size, varying from 1.4×10^{-27} to 72.4×10^{-27} esu as the particles grow from 2 to 9 nm in diameter. These values of β are among the largest observed for solution samples. Moreover, the values of β normalized per unit volume (β/V) and per CdS pair are observed to increase with decreasing of size, leading to an enhancement of about 1 order of magnitude in β for 2 nm nanocrystals in comparison with bulk CdS. This observation can be explained by the enhancement of both bulk and surface contributions. The enhancement of the bulk contribution is ascribed to quantum confinement effects on the volume normalized oscillator strengths, which increase with decreasing particle size because of the enhanced spatial overlap between the electron and hole wave functions. The surface contribution can be expected to become more significant as the size decreases, because of the larger surface/bulk ratio, and can be enhanced by several effects, particularly surface polarization. The bulk contribution seems to be the dominating one even for smaller sizes (i.e., 2 nm).

Acknowledgment. The authors are grateful to Dr. C.A.P. Leite and Prof. F. Galembeck (Unicamp–Brazil) for transmission electron microscopy measurements. Financial support from the Brazilian agencies CNPq and PADCT is gratefully acknowledged.

References and Notes

- (1) For a review, see: Gaponenko, S. V. *Optical Properties of Semiconductor Nanocrystals*; Cambridge University Press: Cambridge, U.K., 1998.
- (2) Brus, L. *Appl. Phys. A* **1991**, *53*, 465.
- (3) Alivisatos, A. P. *J. Phys. Chem.* **1996**, *100*, 13226.
- (4) Jakubczyk, D.; Shen, Y.; Lal, M.; Friend, C.; Kim, K. S.; Swiatkiewicz, J.; Prasad, P. N. *Opt. Lett.* **1999**, *24*, 1151.
- (5) Bruchez, M., Jr.; Moronne, M.; Gin, P.; Weiss, S.; Alivisatos, A. P. *Science* **1998**, *281*, 2013.
- (6) Shan, W. C. W.; Nie, S. *Science* **1998**, *281*, 2016.
- (7) Lacoste, T. D.; Michalet, X.; Pinaud, F.; Chemla, D. S.; Alivisatos, A. P.; Weiss, S. *Proc. Natl. Acad. Sci. U.S.A.* **2000**, *97*, 9461.
- (8) Prasad, P. N.; Williams, D. J. *Introduction to nonlinear optical effects in molecules and polymers*; John Wiley & Sons Inc.: New York, 1991.
- (9) Nakamura, A.; Tokizaki, T.; Akiyama, H.; Kataoka, T. *J. Lumin.* **1992**, *53*, 105.
- (10) Banyai, L.; Hu, Y. Z.; Lindberg, M.; Koch, S. W. *Phys. Rev. B* **1988**, *38*, 8142.
- (11) Yao, H.; Takahara, S.; Mizuma, H.; Kozeki, T.; Hayashi, T. *Jpn. J. Appl. Phys.* **1996**, *35*, 4633.
- (12) Cotter, D.; Burt, M. G.; Manning, R. J. *Phys. Rev. Lett.* **1992**, *68*, 1200.
- (13) Wang, Y.; Herron, N. *J. Phys. Chem.* **1991**, *95*, 5, 525.

- (14) Heping, L.; Liu, B.; Kam, C. H.; Lam, Y.-L.; Que, W.; Gan, L. M.; Chew, C. H.; Xu, G. Q. *Proc. SPIE* **1999**, 3899, 376.
- (15) Li, H. P.; Liu, B.; Kam, C. H.; Lam, Y. L.; Que, W. X.; Gan, L. M.; Chew, C. H.; Xu, G. Q. *Opt. Mater. (Amsterdam)* **2000**, 14, 321.
- (16) Loicq, J.; Torrenti, C.; Renotte, Y. L. M.; Calberg, C.; Delplancke, J. L.; Lion, Y. F. *Proc. SPIE* **2000**, 4089, 815.
- (17) Yumashev, K. V.; Posnov, N. N.; Denisov, I. A.; Prokoshin, P. V.; Mikhailov, V. P.; Gurin, V. S.; Prokopenko, V. B.; Alexeenko, A. A. *J. Opt. Soc. Am. B* **2000**, 17, 572.
- (18) Malyarevich, A. M.; Yumashev, K. V.; Posnov, N. N.; Mikhailov, V. P.; Gurin, V. S.; Prokopenko, V. B.; Alexeenko, A. A.; Melnichenko, I. M. *J. Appl. Phys.* **2000**, 87, 212.
- (19) Klimov, V. I. *J. Phys. Chem. B* **2000**, 104, 6112.
- (20) Aktsipetrov, O. A.; Baranova, I. M.; Dubinina, E. M.; Elovikov, E. S.; Elyutin, P. V.; Esikov, D. A.; Nikulin, A. A.; Fominykh, N. N. *Phys. Lett. A* **1986**, 117, 239.
- (21) Aktsipetrov, O. A.; Elyutin, P. V.; Nikulin, A. A.; Ostrovskaya, E. A. *Phys. Rev. B* **1995**, 51, 17591.
- (22) Fu, D.-G.; Li, M.; Wang, X.; Cheng, J.-Q.; Yu, Z.; Lu, Z.-H.; Liu, J.-Z.; Cui, Y.-P. *Supramol. Sci.* **1998**, 5, 495.
- (23) Wang, X.; Zhang, Y.; Shen, Y.; Li, M.; Fu, D.-G.; Lu, Z.-H.; Cui, Y. *Proc. SPIE* **2000**, 3937, 123.
- (24) Zhang, Y.; Wang, X.; Fu, D.-G.; Liu, J. Z.; Lu, Z. H. *Chin. Chem. Lett.* **2000**, 11, 375.
- (25) Brysch, A.; Bour, G.; Neuendorf, R.; Kreibig, U. *Appl. Phys. B* **1999**, 68, 447.
- (26) Santos, B. S.; Pereira, G. A. L.; Petrov, D. V.; de Mello Donegá, C.; *Optics Commun.* **2000**, 178, 187.
- (27) Jacobsohn, M. and Banin, U. *J. Phys. Chem.* **2000**, 104, 1.
- (28) Henglein, A.; Gutiérrez, M. *Ber. Bunsen-Ges. Phys. Chem.* **1983**, 87, 852.
- (29) Spanhel, L.; Haase, M.; Weller, H.; Henglein, A. *J. Am. Chem. Soc.* **1987**, 109, 5649.
- (30) Kumar, A.; Janata, E.; Henglein, A. *J. Phys. Chem.* **1988**, 92, 2587.
- (31) Weller, H. *Angew. Chem., Int. Ed. Engl.* **1993**, 32, 41.
- (32) Van Dijken, A.; Makkinje, J.; Meijerink, A. *J. Lumin.* **2001**, in press.
- (33) Terhune, R. W.; Maker, P. D.; Savage, C. M. *Phys. Rev. Lett.* **1965**, 14, 681.
- (34) Hendrix, E.; Clays, K.; Persoon, A. *Acc. Chem. Res.* **1998**, 31, 675.
- (35) Flipse, M. C.; de Jonge, R.; Wounderberg, R. H.; Marsman, A. W.; van Warlee, C. A.; Jennekens, L. W. *Chem. Phys. Lett.* **1995**, 245, 297.
- (36) Song, N. W.; Kang, T.-I.; Jeoung, S. C.; Jeon, S.-J.; Cho, B. R.; Kim, D. *Chem. Phys. Lett.* **1996**, 261, 301.
- (37) Turro, N. J. *Modern molecular photochemistry*; Benjamin: New York, 1978; p 105.
- (38) Madelung, O.; Martienssen, W., Eds.; *Landolt-Bornstein. Numerical data and functional relationships in science and technology*, Springer-Verlag: Berlin, 1988; Volume III-17b, pp 61–115 (ZnS), 166–194 (CdS), 202–221 (CdSe).
- (39) Clays, K.; Persoon, A. *Phys. Rev. Lett.* **1991**, 66, 2980.
- (40) Clays, K.; Persoon, A. *Rev. Sci. Instrum.* **1992**, 63, 3285.
- (41) Morrison, I. D.; Denning, R. G.; Laidlaw, W. M.; Stammers, M. A. *Rev. Sci. Instrum.* **1996**, 67, 1445.
- (42) Vance, F. W.; Lemon, B. I.; Hupp, J. T. *J. Phys. Chem. B* **1998**, 102, 10091.
- (43) Vossmeier, T.; Katsikas, L.; Giersig, M.; Popovic, I. G.; Diesner, K.; Chemseddine, A.; Eychmüller, A.; Weller, H. *J. Phys. Chem.* **1994**, 98, 7665.
- (44) Tittel, J.; Göhde, W.; Koberling, F.; Basché, Th.; Kornowski, A.; Weller, H.; Eychmüller, A. *J. Phys. Chem. B* **1997**, 101, 3013.
- (45) (a) Edamura, T.; Muto, J. *Thin Solid Films* **1993**, 226, 135. Henglein, A.; Gutiérrez, M. *Ber. Bunsen-Ges. Phys. Chem.* **1983**, 87, 852. Qi, L.; Ma, J.; Cheng, H.; Zhao, Z. *Colloids Surf. A* **1996**, 111, 195. Huang, J.; Lianos, P. *Langmuir* **1998**, 14, 4342. (b) Berger, L. I. *Semiconductor Materials*; CRC Press: Boca Raton, FL, 1994.
- (46) Oudar, J. L.; Chemla, D. S. *J. Chem. Phys.* **1977**, 66, 2664.
- (47) Rajh, T.; Micic, O. I.; Lawless, D.; Serpone, N. *J. Phys. Chem.* **1992**, 96, 4633.
- (48) Majetich, S. A.; Carter, A. C. *J. Phys. Chem.* **1993**, 97, 8727.
- (49) Dadap, J. I.; Shan, J.; Eisenthal, K. B.; Heinz, T. F. *Phys. Rev. Lett.* **1999**, 83, 4045.
- (50) Sutherland, R. L. *Handbook on nonlinear optics*; Marcel Dekker Inc.: New York, 1996.
- (51) Brus, L. E. *J. Chem. Phys.* **1984**, 80, 4403.
- (52) van Dijken, A.; Janssen, A. H.; Smitsmans, M. H. P.; Vanmaekelbergh, D.; Meijerink, A. *Chem. Mater.* **1998**, 10, 3513.
- (53) Banyai, L.; Gilliot, P.; Hu, Y. Z.; Koch, S. W. *Phys. Rev. B* **1992**, 45, 14136.
- (54) Shen, Y. R. *Appl. Phys. B* **1999**, 68, 295.
- (55) Bloembergen, N. *Appl. Phys. B* **1999**, 68, 289.